Experimental Eye Research 150 (2016) 34–43

Contents lists available at ScienceDirect

Experimental Eye Research

journal homepage: www.elsevier.com/locate/yexer

Research article

Glial coverage in the optic nerve expands in proportion to optic axon loss in chronic mouse glaucoma

Alejandra Bosco [a, *], Kevin T. Breen [a], Sarah R. Anderson [a], Michael R. Steele [a], David J. Calkins [b], Monica L. Vetter [a]

[a] Department of Neurobiology and Anatomy, School of Medicine, University of Utah, Salt Lake City, UT 84112, United States
[b] Department of Ophthalmology and Visual Sciences, Vanderbilt University Medical Center, Nashville, TN 37205, United States

ARTICLE INFO

Article history:
Received 21 July 2015
Received in revised form
21 December 2015
Accepted in revised form 23 January 2016
Available online 3 February 2016

Keywords:
Glaucoma
Neurodegeneration
Optic nerve
Axon loss
Remodeling
Gliosis
Microglia
Segmentation

ABSTRACT

Within the white matter, axonal loss by neurodegeneration is coupled to glial cell changes in gene expression, structure and function commonly termed gliosis. Recently, we described the highly variable expansion of gliosis alebosco@neuro.utah.edu in degenerative optic nerves from the DBA/2J mouse model of chronic, age-related glaucoma. Here, to estimate and compare the levels of axonal loss with the expansion of glial coverage and axonal degeneration in DBA/2J nerves, we combined semiautomatic axon counts with threshold-based segmentation of total glial/scar areas and degenerative axonal profiles in plastic cross-sections. In nerves ranging from mild to severe degeneration, we found that the progression of axonal dropout is coupled to an increase of gliotic area. We detected a strong correlation between axon loss and the aggregate coverage by glial cells and scar, whereas axon loss did not correlate with the small fraction of degenerating profiles. Nerves with low to medium levels of axon loss displayed moderate glial reactivity, consisting of hypertrophic astrocytes, activated microglia and normal distribution of oligodendrocytes, with minimal reorganization of the tissue architecture. In contrast, nerves with extensive axonal loss showed prevalent rearrangement of the nerve, with loss of axon fascicle territories and enlarged or almost continuous gliotic and scar domains, containing reactive astrocytes, oligodendrocytes and activated microglia. These findings support the value of optic nerve gliotic expansion as a quantitative estimate of optic neuropathy that correlates with axon loss, applicable to grade the severity of optic nerve damage in mouse chronic glaucoma.

1. Introduction

The progressive decline and loss of optic nerve axons is characteristically associated with vision loss in all types of glaucoma (Casson et al., 2012). This neurodegenerative disease of the retina and optic nerve targets the retinal ganglion cells (RGCs), causing deterioration and destruction of their axons and somata through pathogenic mechanisms that are still unresolved (Quigley, 2011). Axonopathy is progressive and heterogeneous in multiple experimental models of glaucoma (Calkins, 2012; Nickells et al., 2012; Vidal-Sanz et al., 2012). Axonal degeneration is sectorial and asynchronous in models of induced intraocular pressure elevation (Salinas-Navarro et al., 2010; Soto et al., 2011), as well as in the DBA/2J mouse model of inherited, chronic glaucoma (Howell et al., 2007a; John et al., 1998; Schuettauf et al., 2004). Early in DBA/2J glaucoma, sparse degenerative axonal profiles are interspersed within nerves with preserved axon densities, and as disease advances, there is progressive increase in axon degeneration and loss that culminates in axon depletion and nerve scarring (Crish et al., 2010; Inman et al., 2006; Libby et al., 2005a). Given the variable severity and progressive nature of glaucomatous optic nerve degeneration, the assessment of nerve damage in animal models of glaucoma is largely based on grading or quantifying the numbers of persistent axons (reviewed in Nuschke et al., 2015).

Evaluation of optic axon decline and loss is key in rodent models of acute and chronic glaucoma that are used to define mechanisms of RGC and axonal degeneration, and potential neuroprotection. However, this poses challenges due to asynchronous and variable distribution of axon loss and atrophy. Axon drop out can be diffuse and uniform across the entire nerve (Sappington et al., 2010), focal and heterogeneous between fascicles (Morrison et al., 1997), or a

* Corresponding author.
E-mail address: alebosco@neuro.utah.edu (A. Bosco).

http://dx.doi.org/10.1016/j.exer.2016.01.014
0014-4835/

combination of both topographies, as in the DBA/2J model (Schlamp et al., 2006). Direct counting of the number of persistent axonal profiles in semithin nerve cross-sections is the standard and most accurate method to determine glaucomatous axon loss, and much effort continues to be devoted to perfecting this analysis (Nuschke et al., 2015). In rodent models of glaucoma, actual axon counts in light micrographs are performed manually or by semi-automated analysis in nerve subareas distributed in a fixed patterned or within zones selected for their uniform damage (Buckingham et al., 2008; Chauhan et al., 2006; Chen et al., 2011; Crish et al., 2010; Ebneter et al., 2010, 2012; Howell et al., 2007a, 2011; Inman et al., 2006; Isaacs et al., 2014; Jia et al., 2000; Joos et al., 2010; Mabuchi et al., 2003; Marina et al., 2010; May and Mittag, 2006; Sappington et al., 2010; Scholz et al., 2008; Templeton et al., 2014). Alternatively, glaucomatous optic nerves are visually scored by degree and expanse of axon loss, damage, gliosis and scarring by trained observers (Chidlow et al., 2011). This method is commonly applied to grade optic nerve pathology in the DBA/2J mouse strain (Anderson et al., 2005; Harder et al., 2012; Howell et al., 2007b, 2012; Libby et al., 2005a; Pelzel et al., 2012; Schlamp et al., 2006; Son et al., 2010), and is complemented by estimation of the proportion of degenerative axonal profiles (Crish et al., 2010; Howell et al., 2012). Overall, defining disease stage and severity in glaucoma depends on accurate detection and estimation of the variable levels and patterns of axonal degeneration and loss in the optic nerve.

In human and experimental glaucoma, the progressive damage of optic axons is paralleled by gliosis (Anderson et al., 2005; Bosco et al., 2015; Crish et al., 2010; Dai et al., 2012; Hernandez, 2000; Libby et al., 2005a; Lye-Barthel et al., 2013; Qu and Jakobs, 2013; Sappington et al., 2010; Schlamp et al., 2006; Sofroniew, 2009; Son et al., 2010; Sun and Jakobs, 2012; Sun et al., 2009; Yang et al., 2012). Degenerating optic axons are replaced by reactive glial cells, infiltrating cells and extracellular matrix within atrophic nerve areas, in both human patients and in primate models (Jonas et al., 1995; Quigley et al., 1982; Radius and Pederson, 1984). In DBA/2J mice, severely degenerative nerves show extensive gliosis and scarring after 8 months of age, while the number of degenerating axon profiles more than doubles from 3 to 13 months of age (Crish et al., 2010; Schlamp et al., 2006). These conspicuous features have been useful for nerve damage grading (Anderson et al., 2005). However, the relative expansion of total glial territories as axons vacate the glaucomatous optic nerve has not been used as a proxy for axonal neurodegeneration.

In a recent study, we detected a highly variable distribution of optic nerve gliosis across DBA/2J mice (Bosco et al., 2015). Here, using this well-established model of chronic glaucoma, we evaluated whether the global expansion of glial and scarred nerve territories provides a quantifiable estimate of total axonal loss. For this purpose, we analyzed DBA/2J optic nerves representative of healthy, moderate and severe glaucoma, as well as Gpnmb$^{+/+}$ DBA/2J control mice. We quantified and mapped axon density by semiautomated counting methods, and in the same nerve cross-sections we applied image segmentation methods to isolate and measure degenerative axonal profiles and nerve area occupied by glial cells and scar tissue. These two methods of analysis of glaucomatous optic nerve degeneration, allowed us to detect a significant positive correlation between the expansion of nerve area occupied by glial cells and the reduction in mean axonal density. Applying segmentation analysis of nerve glial/scar areas and highly degenerative axons to a large cohort of DBA/2J optic nerves, we provide evidence that this semiquantitative method represents a practical and sensitive gauge to score progressive and variable glaucomatous pathology.

2. Materials and methods

2.1. Mice

DBA/2J and non-glaucoma control Gpnmb$^{+/+}$ DBA/2J were bred and housed at the University of Utah (females aged 10–11 months; Figs. 4–5), introducing new breeder mice purchased from Jackson Laboratories (Bar Harbor, ME) twice a year to prevent genetic drift. Additionally, DBA/2J mice (males and females aged 7, 12 and 13 months; Figs. 1–3) were obtained from P.J. Horner (University of Washington Harborview Medical Center, Seattle, WA). All mice were maintained in sterile conditions, on 12/12 light/dark cycles, and fed standard rodent diet. All animal protocols were approved by the local IACUC, and experiments performed in accordance with the ARVO Statement for the Use of Animals in Ophthalmic and Vision Research.

2.2. Nerve histopathology

All optic nerves were collected from mice after transcardial perfusion with 4% paraformaldehyde (PFA) and overnight post-fixation within the exposed orbit, prepared as two pieces (each 1–1.5-mm in length), cut from the postlaminar region. One nerve segment was processed for 1- to 2-μm plastic cross-sections, stained with toluidine-blue and paraphenylenediamine (PPD) to increase contrast for light microscopy, and the contiguous segment was prepared for gelatin embedding, cross-cryosectioning, immunofluorescence and confocal imaging (see below). For plastic embedding, we used previously described processing methods (Calkins et al., 2005; Inman et al., 2006; Sappington et al., 2003), with slight optimization (see Supplemental Methods for detailed protocol).

2.3. Axon counts in light microphotographs

Axon counts for individual optic nerves were obtained as described previously (Buckingham et al., 2008; Crish et al., 2010; Inman et al., 2006; Joos et al., 2010; Sappington et al., 2010). Briefly, a single, plastic cross-section was imaged in its entirety for each nerve by creating a montage of 20–25 adjacent frames using a 100× oil-immersion objective, differential interference contrast optics (Provis AX70; Olympus, Melville, NY), a motorized stage and a digital charge-coupled device (CCD) camera. Image montages were minimally processed for contrast- and edge-enhancing using macro routines (ImagePro; Media Cybernetics, Silver Spring, MD). All axons with an identifiable myelin sheath were counted in each frame at 1,000× digital magnification using an additional macro routine. The axon density was calculated as the number of axons divided by frame area, and the axon density for each nerve was estimated as the mean of densities across frames.

2.4. Segmentation analysis of total glia/scar area and degenerative axon profiles

To identify and measure the relative nerve area corresponding to glial cells and highly degenerative axons, observers masked to nerve identity and axon counts used image segmentation methods recently described (Bosco et al., 2015). First, two observers with expertise in optic nerve histopathology, glaucomatous pathology and image analysis worked together to optimize intensity–threshold parameters to consistently isolate nerve areas occupied by all glial cell types, scar tissue, degenerative axons, blood vessels and meninges, which are explained in detail (Supplemental Methods). Nerve glial and scar areas are prominent and easily recognizable, requiring only minimal manual refinement to include astrocyte

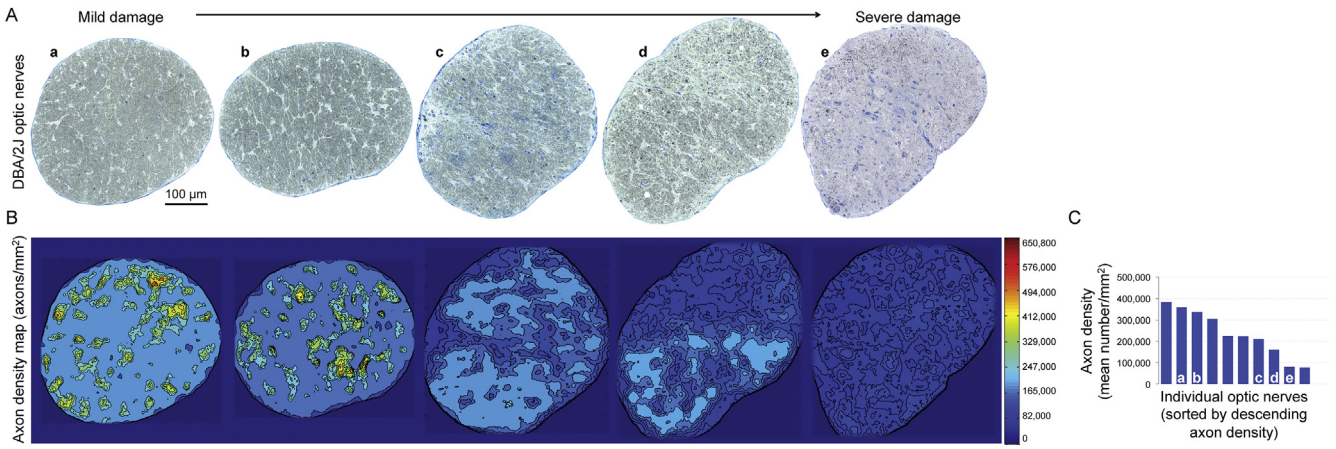

Fig. 1. Decline in axon density is heterogeneous in distribution and levels in adult DBA/2J optic nerves. (**A**) Light microscopy images of DBA/2J optic nerve cross-sections presented as stitched multipoint images acquired at high-resolution. Individual nerves were selected to represent increasing severity of neuropathy at 7 (a), 12 (b–d) and 13 (e) months of age. (**B**) Corresponding spatial maps of axon density, numbers/mm^2, color-coded scale shown at far right), illustrate the variability in distribution and levels of axonal numbers across the same optic nerves. (**C**) Bar graph representing the mean axon density per individual optic nerve cross-section, with individual nerves illustrated in A and B identified with a letter over their corresponding bar. Scale bars: 100 µm.

processes with relatively low contrast that are missed by segmentation. Degenerative axons, in the other hand, present a bigger challenge to threshold analysis due to their variable size and contrast. For this reason, segmentation is limited to axonal profiles with clearly dark myelin and/or axoplasm (dark defined as intensities at least 50% greater than nearby healthy axons). Subsequent observers practiced image segmentation in a set of reference nerves previously analyzed for axon counts, glial and degenerative

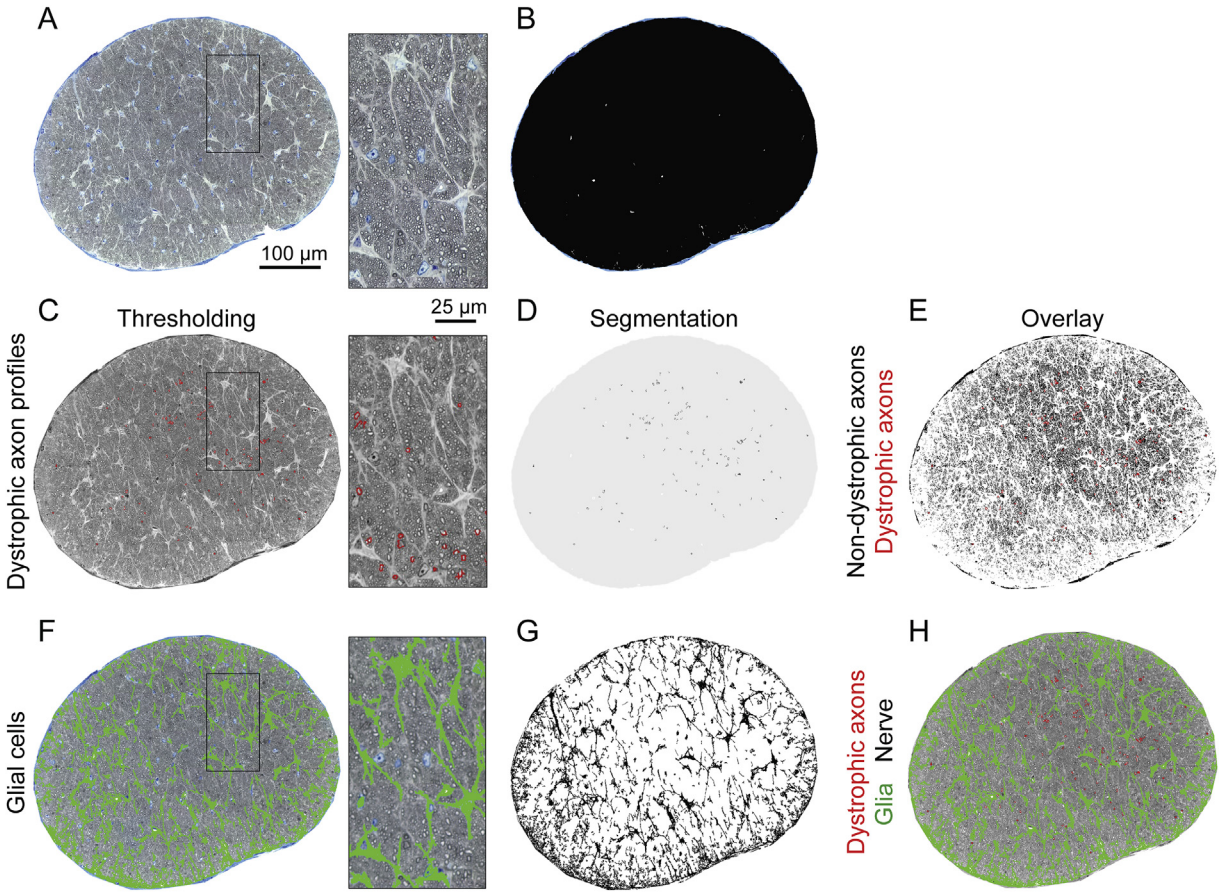

Fig. 2. Image analysis steps used for semi-automatic segmentation and quantification of glial and dystrophic axon coverage in adult DBA/2J optic nerves. (**A**) Light microscopy image of the retro-orbital optic nerve, obtained by montage of multiple high-resolution images spanning a single semithin cross-section. (**B**) Segmented total nerve area excluding the lumen of major blood vessels and the meninges. (**C**) The thresholded degenerative axons included profiles with abnormally dark axoplasm and/or myelin sheets (red areas). (**D**) Dystrophic axons segmented into a quantifiable binary mask. (**E**) Dystrophic axons were identifiable by their high contrast due to PPD staining, and were amenable for quantification (red profiles), while intact axons were inconsistently detectable by segmentation and shown here only for illustration (black profiles). (**F**) (**G**) Thresholded glial cells and processes (green areas) were segmented for the entire nerve. (**H**) Overlay of all three segmented areas used for analysis of nerve degeneration. Scale bar: 100 µm.

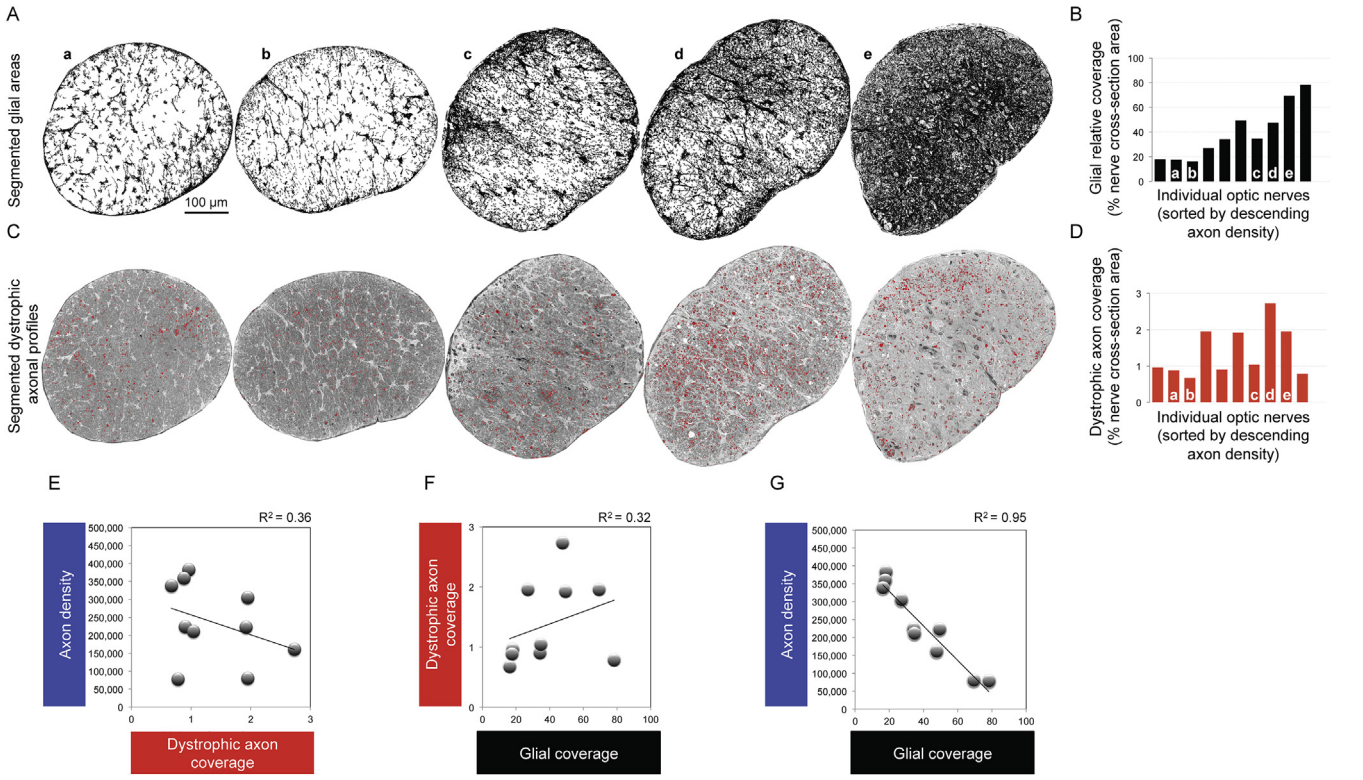

Fig. 3. Glial coverage expands in correlation to progressive axonal loss, while neither glial coverage nor axon loss correlate with axon dystrophy. (**A**) Binary masks of the total glial cell and/or scar area obtained by segmentation of the same nerves (a through e) analyzed in Fig. 1. The aggregate glial cell coverage increases with the severity of pathology in the selected nerves, noticeably within focal gliotic areas (nerves c and d), and as an extensive scar region (nerve e). (**B**) Bar graph representing the percent area covered by glia in individual nerve cross-sections, sorted by descending axonal density (as in Fig. 1C). (**C**) For the same nerves, the segmented dystrophic axons (red areas) are shown overlaid on the original nerve image shown in black and white, to improve observation. (**D**) Bar graph representing the percent area covered by degenerative axon profiles in the same nerve cross-sections, sorted by descending axonal density. Scatterplot graphs of the correlation analysis for (**E**) dystrophic axon coverage versus mean axon density, (**F**) relative glial area per nerve versus relative area of total dystrophic axons, and (**G**) relative glial area per nerve versus mean axon density. R^2 values are provided in each graph and indicated with a solid line. Scale bars: 100 µm.

axon segmentation and coverage, representative of non-glaucoma ($Gpnmb^{+/+}$ DBA/2J nerves with >60,000 axons) and three levels of glaucomatous damage (DBA/2J nerves with >60,000, <30,000 and < 10,000 axons). Supervised training concluded when threshold analysis resulted in low variability with the reference analysis (<5%; data not shown), after minimal manual refinement of segmented areas. Final analysis was performed by researchers blind to nerve condition, who generated binary overlays representing glial and highly degenerative axonal compartments, and then calculated their area relative to the nerve cross-sectional area.

2.5. Nerve immunofluorescence and confocal microscopy

A segment of postlaminar region for the same optic nerves used for nerve histopathology analysis was prepared for cryosections and immunofluorescence as described (Bosco et al., 2011, 2015). In brief, eyes were cryoprotected with 20% sucrose, embedded in gelatin and cross-cryosectioned (16 µm). Nerve cryosections were double-immunostained with mouse anti-GFAP conjugated with Cy3 (1:2,000, C9205, Sigma, St. Louis, MO) and rabbit anti-Iba1 (1:400, 019-19741, Wako, Richmond VA) or rabbit anti-Olig2 (1:750, AB9610, Millipore, Temecula, CA), which were incubated for 3 days at 4 °C, or omitted in negative control slides. Secondary Alexa-conjugated antibodies (donkey anti-mouse or rabbit 488 or 555 or 647 nm, 1:400) were incubated in 1% BSA for 2 h at room temperature. Slides were mounted with Fluoromount-G (Southern Biotech, Birmingham, AL) and imaged by confocal microscopy (A1 system, Nikon, Melville, NY). Each nerve was imaged with 20× dry objective and optical zoom to a final resolution of 0.42 µm/px. The final image spanning the entire nerve cross-section was stitched from multiple single images spanning 10 µm of each section, with a 0.8 µm-z step using the Scan Large Image function (NIS-Elements, Nikon).

2.6. Statistic analysis

Correlations were calculated by two-tailed Pearson product moment test and verified by polynomial regression analysis, and considered significant when $p < 0.01$. Both statistical tests were performed with SigmaPlot (Systat Software Inc., San Jose, CA).

3. Results

3.1. Optic axon loss is highly variable in magnitude and topography in DBA/2J nerves

As a first step to analyze parallel changes in axon degeneration and gliosis in glaucomatous optic nerves, we assessed axon loss in a cohort of DBA/2J mice representative of the variable optic neuropathy reported for this strain (Inman et al., 2006; Libby et al., 2005a). We compared the levels and patterns of axonal density in 10 healthy nerves and degenerative nerves from mice aged 7, 12 and 13 months (n = 2, 6 and 2, respectively). Using light-microscopy images collected as a montage spanning entire semi-thin plastic nerve cross-sections (Fig. 1A), we quantified the number of axons for the entire nerve area, and built axon-density maps by tiling axon counts across frames (Fig. 1B). Healthy optic nerves

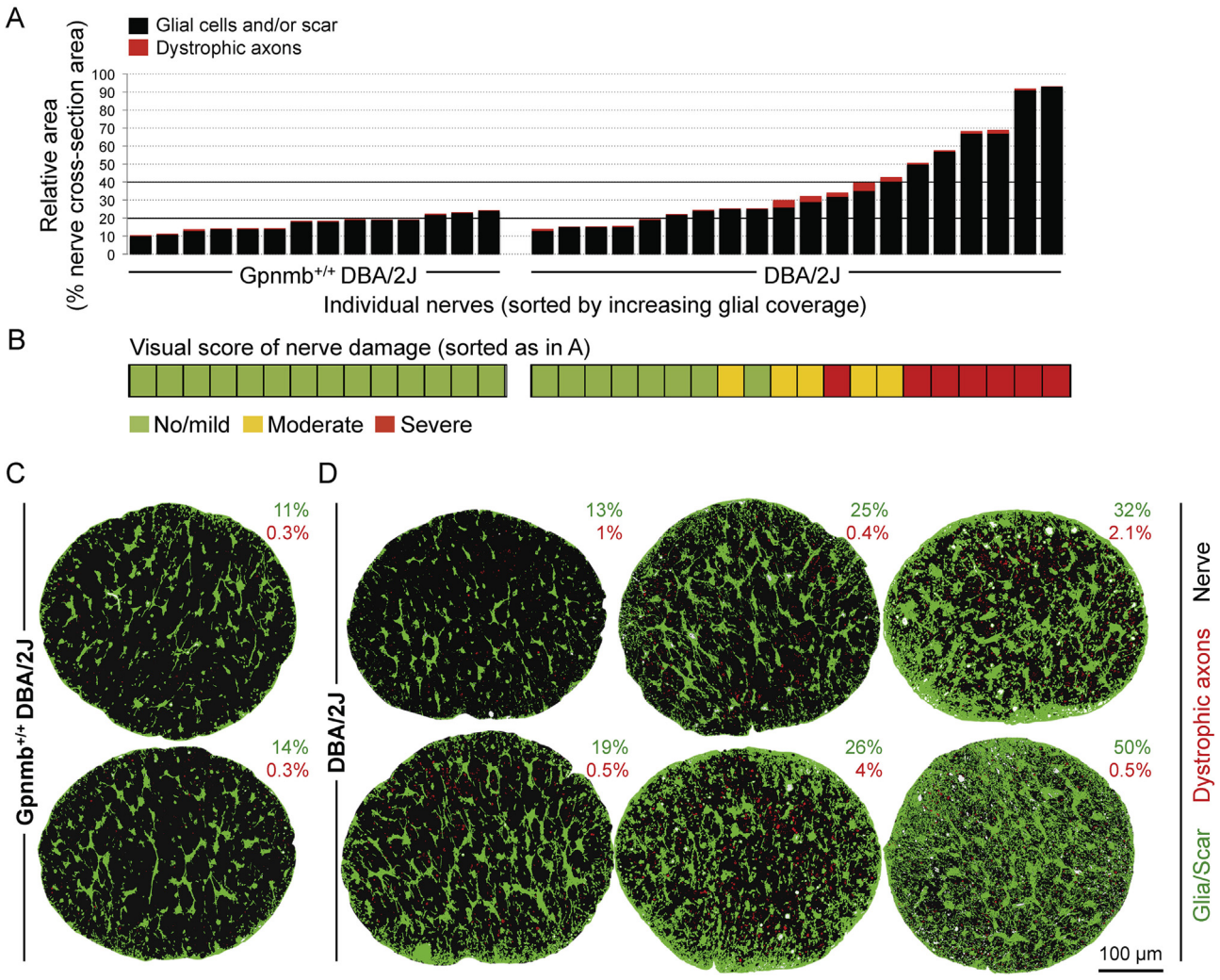

Fig. 4. The relative coverage of glia and degenerative axons serves as an objective parameter to assess the severity of glaucomatous nerve damage in DBA/2J mice. (**A**) Plot of individual optic nerves from 10-month-old *Gpnmb*$^{+/Sjl}$ DBA/2J and DBA/2J mice, showing the relative coverage of glia/scar (black) and dystrophic axons (red), and sorted by ascending glial coverage. (**B**) Visual scoring damage in the same nerves, as mild (green), moderate (yellow) and severe (red). (**C and D**) Gallery of overlaid masks of segmented glia/scar (green) and degenerative axons (red) for representative *Gpnmb*$^{+/Sjl}$ DBA/2J nerves and DBA/2J nerves, with relative areas for glia/scar and dystrophic axons indicated for each (top and bottom percent, respectively). Scale bar: 50 µm.

with mild or undetectable axonal loss showed focal fascicular areas with high axon density (400,000–600,000 axons/mm^2), embedded within a large, continuous territory of evenly moderate axonal densities (~250,000 axons/mm^2), both at 7 or 12 months of age (Fig. 1B, nerves a and b, respectively). Nerves with intermediate axonal loss, indicative of more advanced stages of disease progression, lacked focal areas with high axon density, and showed large territories of moderate to low axon densities (~100,000–200,000 axons/mm^2), spanning most or part of the nerve at 12 months of age (Fig. 1B, nerves c and d, respectively). Nerves with severe glaucoma at 13 months of age, exhibited low to very low axon densities (<150,000 axons/mm^2), widespread throughout the entire nerve area (Fig. 1B, nerve e).

Mean axon density for individual nerves (n = 10) provides a global measure of glaucoma severity, and demonstrates the large variability in stages of disease progression (Fig. 1C), consistent with multiple reports on the variable severity of optic neuropathy in the DBA/2J age-related glaucoma (Inman et al., 2006; Libby et al., 2005a). The analyzed nerves display diverse patterns of degeneration and a wide range of mean axon densities, varying almost 5× from ~380,000 to 80,000 axons/mm^2 (Fig. 1C).

3.2. Nerve areas occupied by dystrophic axons and glia can be isolated and quantified by image thresholding and segmentation

The deterioration and loss of optic axons during chronic glaucomatous degeneration in DBA/2J mice is concomitant with changes in reactivity, distribution or numbers of their supporting glial neighbors (Anderson et al., 2005; Schlamp et al., 2006). We recently showed that the segmentation of optic nerve glial and scar territories, and quantification of their relative area provide an objective measure of degeneration severity (Bosco et al., 2015). Here, we sought to define the possibility of evaluating axon loss by quantifying the expansion of degenerative axonal and non-axonal territories. We used the same cohort of DBA/2J optic nerves for which we mapped reductions in axon density (Fig. 1C) to estimate their corresponding glial and dystrophic axon coverage. To identify the relative nerve area occupied by glia and/or scar tissue, as well as degenerative axonal profiles, we used high-resolution, light images of the retro-orbital nerve segment (1–1.5 mm post-lamina; 1-µm-thick cross-sections; Fig. 2A), and applied threshold-based image analysis to segment nerve areas of diverse intensity (Suppl. Fig. 1) as explained in Methods and Supplementary Methods.

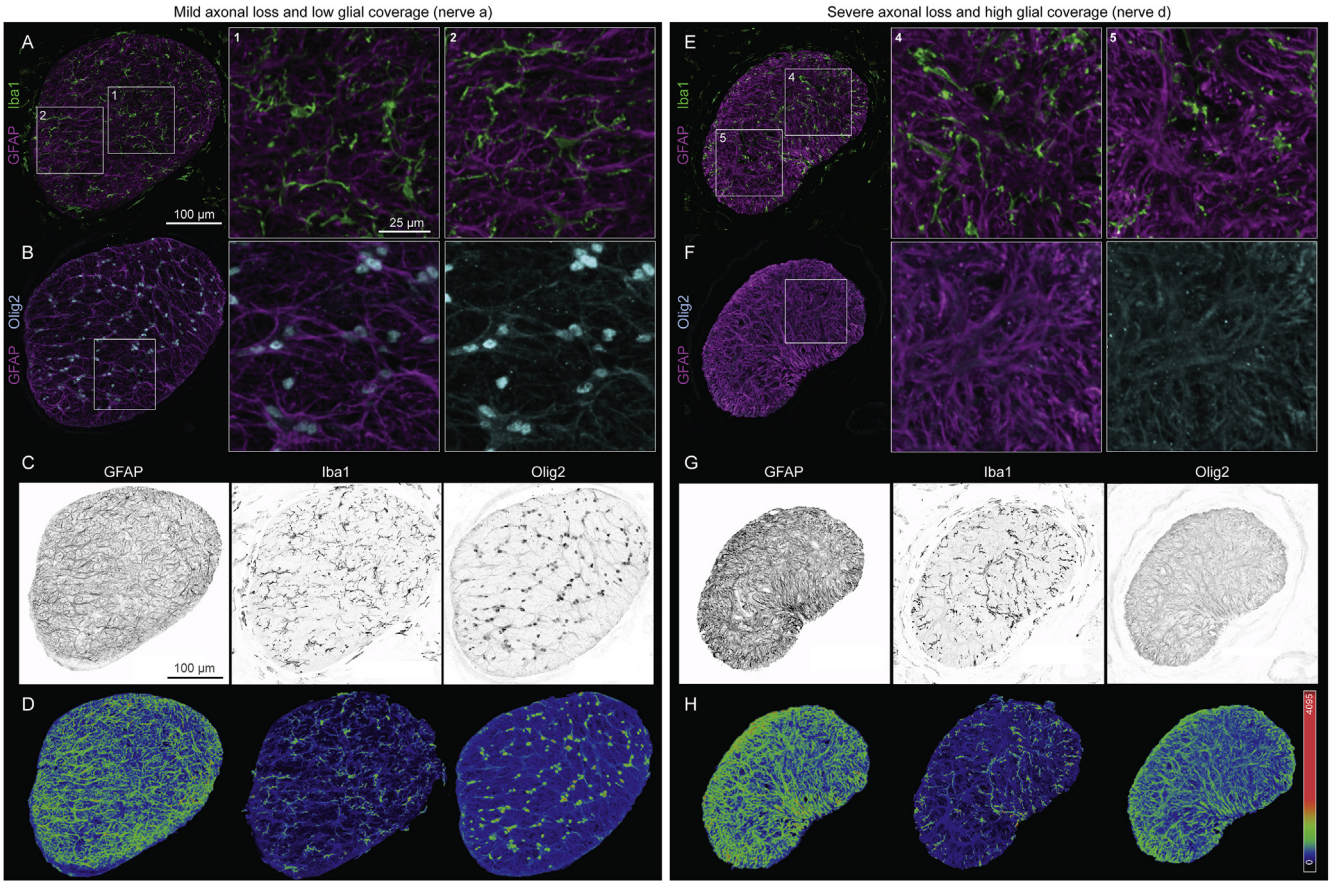

Fig. 5. Remodeling and reactivity of optic nerve astrocytes, microglia and oligodendrocytes associated with the expansion of glial cell and/or scar coverage. Confocal images of astrocytes, microglia and oligodendrocytes in two nerves representative of mild (**A-D**) and severe degeneration (**E-H**) (see Figs. 1B and 3A). Images are 10 µm-maximal intensity projections of cryosections double-immunostained for GFAP and Iba1 (**A** and **E**) or Olig2 (**B** and **F**). High-magnification views of nerve sectors framed in A, B, E and F. (**C** and **G**) Single-channel views of GFAP, Iba1 and Olig2 immunostainings, shown in black and white, to illustrate coverage. (**D** and **H**) Corresponding pseudocolor view to detect variations in signal levels (intensity scale shown far right in H). Scale bar: 100 µm (A–H) and 25 µm (insets).

Selecting different intensity ranges we defined three binary masks (Fig. 2 and Suppl. Fig. 1), corresponding to: 1) the total nerve area excluding meninges and vessels (Fig. 2B), 2) areas occupied by degenerative axonal profiles (Figs. 2C and D), and 3) areas covered by glial cells and scar tissue (Fig. 2F and G). The segmented degenerative axon profiles included axons of diverse caliber with darkly PPD-stained axoplasm and/or myelin sheaths (defined as those with intensity 50% higher than nearby healthy axons), as well as hollow or vacuolized axons with delaminated or fragmented dark myelin sheaths, both representing highly degenerative axons (Smith et al., 2002).

In comparison, structurally healthy axons were variably detectable by threshold, given their lower contrast (Fig. 2E). Once the intensity range for semiautomated image segmentation was optimized, we refined segmented areas manually, to exclude small, artifactual holes usually affecting the peripheral nerve area, closest to the meninges) and the lumen and wall of blood vessel lumina. This image segmentation analysis generates masks corresponding to glia, gliotic cells and scars, and to highly degenerating axons for individual nerves, which are quantifiable by standard image analysis functions.

3.3. *Optic nerve glial coverage expands in correlation to progressive axonal loss*

Optic nerve degeneration in DBA/2J mice is characterized by the progressive and subtle decline and loss of individual axons, which associates with increasing reactivity of glial cells and scarring of nerve areas depleted of axons (Anderson et al., 2005; Schlamp et al., 2006). Here, following up our detection of the variable expansion of glial territories in DBA/2J optic nerves as a quantifiable readout of nerve damage (Bosco et al., 2015), we examined the quantitative relationship between axonal degeneration or loss and the concomitant remodeling in glial coverage. For this, in the same cohort of DBA/2J optic nerves that were analyzed for axonal density (Fig. 1), we segmented the relative area occupied by glial cells and/or scar, and quantified their aggregate coverage (Fig. 3A and B). Regardless of age, healthy nerves (Fig. 3A, a and b) displayed regularly distributed glial cell somata across the entire cross-section. However, nerves with moderate and sectorial axon drop out (Fig. 3A, c and d) showed disorganized and more conspicuous glial cells that clustered within focal areas with increased gliosis. In a nerve with severe and widespread axonal loss (Fig. 3A, e), glial area had coalesced to occupy almost the entire nerve cross-sectional area. The gamut of the relative glial area in optic nerves with increasing axon loss depicted an almost continuous increase in non-axonal territories occupied by glial cells, which spanned less than 20% in nerves with high axonal densities and expanded to near 80% in nerves largely depleted of axons (Fig. 3B), consistent with our previous report (Bosco et al., 2015). These data suggest that the percent of nerve area covered by glial cells and processes increases with the severity of axonal drop out in DBA/2J mouse glaucoma.

In the same nerves, we applied segmentation to identify highly degenerative axons through the entire nerve cross-sectional area (Fig. 3C). To establish the feasibility of segmenting highly degenerative axons with abnormal myelin and/or axoplasm, we independently analyzed a subset of 11 month-old DBA/2J nerves ($n = 8$) by thresholding and by manual counts of degenerative profiles (Suppl. Fig. 2A). The number of highly degenerative axons manually detected per nerve and the number of segmented dystrophic axons for selected samples across the same nerve show strong correlation ($r^2 = 0.98$; Suppl. Fig. 2C), suggesting that thresholding can be used as semiquantitative tool to objectively identify clearly degenerative axons.

The relative nerve area measured for segmented degenerative axonal profiles was low (<1%) in nerves with no or mild axonal loss (Fig. 3C, D a and b), but showed variable increases (2–3%) in nerves with moderate damage (c and d), and tapered off in focal areas or nerves with prevalent axon loss (e). The aggregate area occupied by dystrophic axons showed a large variability in the sample of nerves with a range of axon density loss (Fig. 3D). Interestingly, we detected no correlation between the relative area of the segmented degenerative axonal profiles and either the mean axon density ($r^2 = 0.356$, $p < 0.31$; Fig. 3E) or the relative glial area ($r^2 = 0.319$, $p < 0.37$; Fig. 3F). In contrast, we found a highly significant negative correlation between mean axon density and glial coverage ($r^2 = 0.955$, $p < 0.01$; Fig. 3G). Together, these data indicate that the aggregate area spanned by glial cells in an optic nerve is closely representative of the degree of axonal loss (Cooper et al., 2016).

3.4. Glial and dystrophic axon coverage are sensitive metrics to classify glaucomatous nerve damage

Consistent with the variable age of glaucoma onset and progression in the DBA/2J strain, their optic nerves show diverse levels and spread of axonal degeneration after 10 months of age, including some with no detectable damage (Buckingham et al., 2008; Howell et al., 2012; Inman et al., 2006; John et al., 1998; Libby et al., 2005b; Schlamp et al., 2006). As shown in Fig. 3, individual optic nerves display highly variable coverage by glial cell and/or scar tissue, and contain diverse amounts of degenerative axon profiles (Lye-Barthel et al., 2013; Schlamp et al., 2006). To thoroughly define the validity of measuring glial expansion as a proxy for the severity of glaucomatous optic neuropathy, we compared the relative area occupied by glial cells and by dystrophic axons in a cohort of 10-month-old optic nerves from female DBA/2J ($n = 20$) and Gpnmb$^{+/+}$ DBA/2J mice ($n = 14$), the congenic control strain (Fig. 4). Image segmentation analysis in non-glaucoma *Gpnmb*$^{+/SjJ}$ DBA/2J nerves detected relative glial areas varying from 10 to 24% of the nerve cross-section, and an aggregate area of degenerative axonal profiles representing less than 1% of the nerve area (Fig. 4A). Thus, glaucomatous axonal degeneration and loss were absent in *Gpnmb*$^{+/SjJ}$ DBA/2J optic nerves, although there was occasional damage typical of aging (Howell et al., 2007b).

Consistent with our previous report (Bosco et al., 2015), the cohort of DBA/2J nerves showed a continuum of glial cell and/or scar coverage ranging from 13 to 93% of the nerve area, and degenerative axonal profiles covering less than 1%, and up to 5% of the total nerve cross-sectional area (Fig. 4A). Noticeably, DBA/2J nerves with intermediate levels of gliosis (26–35% relative area) showed the highest proportion of degenerative axonal coverage (2–5%), while nerves with low glial coverage (<20%) or with extensive gliotic areas (>40%) contained a lower proportion of degenerative axon areas (<1 and < 2%, respectively). Based upon these data, we define nerves with no or mild damage as those with glial areas below 20%, moderately damaged nerves as those with glial areas from 20 to 40% with conspicuous degenerating axon profiles (up to 5%), and severely damaged nerves as those with glial/scar areas above 40%.

We compared this to qualitative classification of the same cohorts of nerves by visual scoring of their damage. There was good correspondence for graded nerves with no/mild damage from the *Gpnmb*$^{+/SjJ}$ DBA/2J and DBA/2J strains, as well as DBA/2J nerves with severe damage (Fig. 4B). However, we found that visual scoring was less able to accurately classify glaucomatous nerves with intermediate damage, as these were variably classified as healthy, moderate or severe, likely due to variations in focal versus diffuse axon loss. The spectrum of the spread of nerve glia, gliosis and axonal degeneration in control *Gpnmb*$^{+/SjJ}$ DBA/2J and DBA/2J nerves (Fig. 4C and D) illustrate the usefulness and sensitivity of quantifying their coverage to evaluate severity of glaucomatous damage.

3.5. Optic nerve astrocytes, microglia and oligodendrocytes remodel and become reactive as axonal loss and gliosis expand

Glial cell reactivity, loss and/or proliferation occur during glaucomatous optic nerve degeneration, both at early and late phases of disease progression (Inman et al., 2006; Nakazawa et al., 2006; Son et al., 2010). A number of previous studies on DBA/2J optic neuropathy have provided evidence that gliosis and glial scar formation are coupled with alterations in specific glial cell types (Cooper et al., 2016; Crish et al., 2010; Inman and Horner, 2007; Schlamp et al., 2006; Son et al., 2010). In association with axonal degeneration, after 10 months of age DBA/2J optic nerves show astrocyte reactivity and proliferation, as well as oligodendrocyte apoptosis, while microglial cells show proliferation, activation and increased phagocytic activity (Cooper et al., 2016; Crish et al., 2010; Inman and Horner, 2007; Son et al., 2010). How each optic nerve glial cell type influences axonal neurodegeneration is an active focus of research (Burda and Sofroniew, 2014).

Here, we compared the relative distribution and degree of activation of astrocytes, microglia and oligodendrocytes in nerves with low versus high glial cell/scar coverage, parallel to mild versus severe axonal loss. For this, nerves representative of low or high glial coverage (18 vs. 47% nerves a and d in Fig. 1A) were double-immunostained against GFAP and Iba1 or Olig2, and qualitatively examined for astrogliosis, microglial activation and oligodendrocyte loss by confocal microscopy (Fig. 5). Healthy nerves showed GFAP + astrocytes oriented transversally in a dense mesh overlaid with irregularly interspersed Iba1+ ramified microglia (Fig. 5A), and Olig2+ oligodendrocyte nuclei, mostly clustered with astrocytic somata (Fig. 5B). Although these features were largely uniform across the nerve cross-section, glial cell activation and density showed some variability, detectable as different GFAP and Iba1 levels in astrocytes and microglia with a more reactive cell shape (Fig. 5C and D). Thus, astrocytes displaying morphological signs of hypertrophy and upregulated GFAP colocalized to sectors with activated microglia having enlarged somata, shrunken processes and increased Iba1 expression, and with sparse oligodendrocytes (Fig. 5A, insets 1). Astrocytes with moderate GFAP expression localized to nerve sectors occupied by branched microglia with low Iba1 levels and multiple oligodendrocytes (Fig. 5A, inset 2). The variable levels of GFAP, Iba1 and Olig2 expression across the individual nerve were readily noticeable by intensity map representation (Fig. 5D).

In contrast, nerves with severe degeneration showed extensive glial remodeling throughout the entire cross-section, which was manifest by a dense, disorganized network of astrocytes with upregulated GFAP expression overlapped with variably dense, activated microglial cells (Fig. 5E), and a widespread lack of Olig2+ oligodendrocyte nuclei (Fig. 5F). Corresponding single-channel views (Fig. 5G) and maps of immunofluorescence intensity

(Fig. 5H) reveal widespread astrogliosis, microglial clustering and morphological activation across the cross-section, as well as expression of Olig2 throughout the GFAP + cytoplasmic meshwork of hypertrophic astrocytes (Fig. 5F insets). Cytoplasmic expression of Olig2 in reactive astrocytes has also been reported in various injury models (Buffo et al., 2005; Cassiani-Ingoni et al., 2006; Chen et al., 2008; Magnus et al., 2007). The remodeling observed in astrocytes, microglia and oligodendrocytes suggest that the mesh of reactive astrocytes and activated microglia account in large part for the increased glial coverage during the recession of axonal density, although non-glial cell types or extracellular matrix components likely also contribute to the expanded non-axonal area.

4. Discussion

Neurodegenerative diseases trigger gradual and chronic tissue remodeling, characterized by progressive deterioration and loss of neuronal integrity and a parallel escalation in gliosis (Burda and Sofroniew, 2014; Verkhratsky et al., 2014). In glaucoma, optic nerve axonal degeneration is known to concur with reactivity and/or proliferation of multiple glial cell types (Inman et al., 2011), but no studies have analyzed the global glial expansion as a metric of the severity of optic neuropathy in the context of age-related chronic glaucoma. In the present study we examined the relationship between axon dystrophy or drop out and glial and/or scar coverage in optic nerves from DBA/2J mice and the congenic *Gpnmb*$^{+/SjJ}$ DBA/2J non-glaucoma control strain (Howell et al., 2007b). We described image segmentation methods that allow the isolation and quantification of nerve areas occupied by glial cells and/or scar tissue in healthy nerves and across a spectrum of glaucomatous optic neuropathy. We show a strong negative correlation between mean axonal density and the relative aggregate area of glial cells and/or scar tissue across individual nerves, indicating that glial and/or scar coverage readily and precisely identifies the level of nerve degeneration. Finally, immunostaining analysis of DBA/2J optic nerves representative of mild and severe neuropathy shows that nerve gliosis and scarring results from a combined signature of astrocyte, microglia and oligodendrocyte reactivity and remodeling.

Our findings are consistent with studies in diverse experimental models of glaucoma that have reported a relationship between optic nerve degeneration and diverse measures of glial hypertrophy. For example, loss of RGC axon number or integrity associates with increased number and reactivity of astrocytes (vimentin expression) in DBA/2J mice and following acute ocular hypertension (Son et al., 2010). In addition, phagocytic microglial cells associate with severe axonal and myelin degeneration (Son et al., 2010). Other studies have also found that optic axon loss is associated with significant glial and connective tissue changes (Ebneter et al., 2010; Gottanka et al., 2005; Joos et al., 2010; Mabuchi et al., 2003; May and Mittag, 2006; Sandell and Peters, 2002; Schlamp et al., 2006). However, the relative proportion of glial remodeling relative to axonal degeneration and loss has been less explored during chronic disease progression. We have expanded upon previous findings by quantifying these changes and showing a highly significant negative correlation between mean axon density and glial coverage. Thus, we establish that the amount of glial remodeling and expansion closely mirrors axonal loss, and offers a prominent readout for glaucomatous nerve damage.

Multiple strategies have been developed for estimating the extent of optic nerve damage. The gold standard is direct counting of the number of persistent axonal profiles in semithin nerve cross-sections (Nuschke et al., 2015), however for many labs this is not always feasible or practical. Alternatively, axon counts can be estimated by sampling nerve subareas, but this poses challenges since nerve degeneration can be highly variable across the nerve (Buckingham et al., 2008; Chauhan et al., 2006; Chen et al., 2011; Crish et al., 2010; Ebneter et al., 2010, 2012; Howell et al., 2007a, 2011; Inman et al., 2006; Isaacs et al., 2014; Jia et al., 2000; Joos et al., 2010; Mabuchi et al., 2003; Marina et al., 2010; May and Mittag, 2006; Reynaud et al., 2012; Sappington et al., 2010; Scholz et al., 2008; Teixeira et al., 2014; Templeton et al., 2014). Many studies employ visual grading of optic nerve damage by trained observers, factoring in axon damage and loss, gliosis and glial scarring (Anderson et al., 2005; Chidlow et al., 2011; Crish et al., 2010; Harder et al., 2012; Howell et al., 2007b, 2012; Libby et al., 2005a; Pelzel et al., 2012; Schlamp et al., 2006; Son et al., 2010). However, consistent visual scoring can be challenging due to variations in focal versus diffuse axon loss. We find our strategy of estimating glial expansion to be a useful alternative to these approaches. It can be performed on any high quality light microscopy image of the nerve using standard thresholding and quantification tools available in most image analysis software. The output of the analysis is a semi-quantitative estimate of axon loss across the whole nerve, which allows for fairly straightforward classification of mild, moderate or damaged nerves. As for visual scoring, training is required to reliably define areas of glial coverage and degenerative axon profiles, as we detail in our methods. One limitation of the approach is that thresholding can only reliably detect degenerative axon profiles, with dark abnormal myelin and/or axoplasm, and not early dystrophic ones. Nevertheless, we confirmed that this matches what is detected manually, and posit that it is a partial representation of the extent of axon damage.

We also compared nerves with low versus high glial coverage, parallel to mild versus severe axonal loss, and observed changes in the relative distribution and degree of activation of astrocytes, microglia and oligodendrocytes. Previous studies examining glial responses in glaucoma have described changes in all resident glial cell types. We found that with severe degeneration astrocytes became disorganized and reactive, with upregulated GFAP expression. This is consistent with previous studies showing that astrocytes become reactive and proliferative in DBA/2J nerves undergoing moderate and severe degeneration, as well as shortly after rising intraocular pressure (Crish et al., 2010; Inman and Horner, 2007; Son et al., 2010). There is also substantial remodeling of astrocytes as the nerve degenerates, with reduction of astrocyte area at early stages when dystrophic axons expand, followed by glial expansion with axon loss (Cooper et al., 2016). Interestingly, within the unmyelinated portion of the DBA/2J optic nerve, a subset of laminar astrocytes reduce their coverage concomitant to increasing intraretinal axon loss, due to process reshaping and branch simplification (Lye-Barthel et al., 2013).

When comparing optic nerves with mild versus severe degeneration, we found evidence for loss of Olig2+ nuclei, suggesting either downregulation of Olig2 expression or loss of oligodendrocytes. Oligodendrocyte death has been reported in the DBA/2J optic nerve, and in models of induced ocular hypertension during distinct stages of axonal degeneration (Nakazawa et al., 2006; Son et al., 2010). Interestingly, we observed upregulation of Olig2 in reactive GFAP + astrocytes of degenerative optic nerves. The detection of Olig2 in reactive astrocytes in various injury models has suggested a role in astrogliosis (Buffo et al., 2005; Cassiani-Ingoni et al., 2006; Magnus et al., 2007). Consistent with this, lineage tracing and cell-type-specific mutagenesis studies demonstrated a selective upregulation of Olig2 in astrocytes, which was responsible for their proliferation and reactivity after cortical injury (Chen et al., 2008). Thus, our findings of astroglial expression of Olig2 in severe glaucomatous neuropathy suggest a link to astrocyte responses during optic nerve degeneration.

Finally, we found increased density and activation of microglia

in nerves with more severe degeneration. Microglial activation is detectable in the proximal optic nerves of young DBA/2J mice at pre-degenerative ages (Bosco et al., 2011), while increased phagocytic activity has been assigned to activated microglia in severely degenerative nerves at 10 months of age (Soto et al., 2008). Likewise, reactive microgliosis has been reported in nerves from animals subjected to intraocular pressure elevation (i.e (Johnson et al., 2007; Naskar et al., 2002). Altogether, the collective evidence implies that astrocytes, microglia, oligodendrocytes and infiltrating cells from the circulation are relevant responders and potentially modulators of RGC axonal integrity and decline within the optic nerve and optic nerve head. We now establish a significant quantitative correlation between the expansion of gliosis and axon loss in the DBA/2J mouse strain.

Acknowledgments

The DBA/2J mice used for optic axon counts were kindly provided by Drs. Phillip Horner and Denise Inman (University of Washington), as part of the Catalyst for a Cure consortium (Glaucoma Research Foundation). We thank Cesar O. Romero for technical support with mouse management and tissue processing.This work was supported by the Glaucoma Research Foundation and the Melza M. and Frank Theodore Barr Foundation (Catalyst for a Cure I) to MLV and DJC, and grants from the University of Utah Vision Core (5P30EY014800) and the US National Institute of Healthy (R01EY020878 and R01EY023621) to MLV.

Appendix A. Supplementary data

Supplementary data related to this article can be found at http://dx.doi.org/10.1016/j.exer.2016.01.014.

References

Anderson, M.G., Libby, R.T., Gould, D.B., Smith, R.S., John, S.W., 2005. High-dose radiation with bone marrow transfer prevents neurodegeneration in an inherited glaucoma. Proc. Natl. Acad. Sci. U. S. A. 102, 4566–4571.
Bosco, A., Romero, C.O., Breen, K.T., Chagovetz, A.A., Steele, M.R., Ambati, B.K., Vetter, M.L., 2015. Neurodegeneration severity can be predicted from early microglia alterations monitored in vivo in a mouse model of chronic glaucoma. Dis. Model Mech. 8, 443–455.
Bosco, A., Steele, M.R., Vetter, M.L., 2011. Early microglia activation in a mouse model of chronic glaucoma. J. Comp. Neurol. 519, 599–620.
Buckingham, B.P., Inman, D.M., Lambert, W., Oglesby, E., Calkins, D.J., Steele, M.R., Vetter, M.L., Marsh-Armstrong, N., Horner, P.J., 2008. Progressive ganglion cell degeneration precedes neuronal loss in a mouse model of glaucoma. J. Neurosci. Off. J. Soc. Neurosci. 28, 2735–2744.
Buffo, A., Vosko, M.R., Erturk, D., Hamann, G.F., Jucker, M., Rowitch, D., Gotz, M., 2005. Expression pattern of the transcription factor Olig2 in response to brain injuries: implications for neuronal repair. Proc. Natl. Acad. Sci. U. S. A. 102, 18183–18188.
Burda, J.E., Sofroniew, M.V., 2014. Reactive gliosis and the multicellular response to CNS damage and disease. Neuron 81, 229–248.
Calkins, D.J., 2012. Critical pathogenic events underlying progression of neurodegeneration in glaucoma. Prog. Retin. Eye Res. 31, 702–719.
Calkins, D.J., Sappington, R.M., Hendry, S.H., 2005. Morphological identification of ganglion cells expressing the alpha subunit of type II calmodulin-dependent protein kinase in the macaque retina. J. Comp. Neurol. 481, 194–209.
Cassiani-Ingoni, R., Coksaygan, T., Xue, H., Reichert-Scrivner, S.A., Wiendl, H., Rao, M.S., Magnus, T., 2006. Cytoplasmic translocation of Olig2 in adult glial progenitors marks the generation of reactive astrocytes following autoimmune inflammation. Exp. Neurol. 201, 349–358.
Casson, R.J., Chidlow, G., Wood, J.P., Crowston, J.G., Goldberg, I., 2012. Definition of glaucoma: clinical and experimental concepts. Clin. Exp. Ophthalmol. 40, 341–349.
Chauhan, B.C., Levatte, T.L., Garnier, K.L., Tremblay, F., Pang, I.H., Clark, A.F., Archibald, M.L., 2006. Semiquantitative optic nerve grading scheme for determining axonal loss in experimental optic neuropathy. Investig. Ophthalmol. Vis. Sci. 47, 634–640.
Chen, H., Wei, X., Cho, K.S., Chen, G., Sappington, R., Calkins, D.J., Chen, D.F., 2011. Optic neuropathy due to microbead-induced elevated intraocular pressure in the mouse. Investig. Ophthalmol. Vis. Sci. 52, 36–44.
Chen, Y., Miles, D.K., Hoang, T., Shi, J., Hurlock, E., Kernie, S.G., Lu, Q.R., 2008. The basic helix-loop-helix transcription factor olig2 is critical for reactive astrocyte proliferation after cortical injury. J. Neurosci. Off. J. Soc. Neurosci. 28, 10983–10989.
Chidlow, G., Ebneter, A., Wood, J.P., Casson, R.J., 2011. The optic nerve head is the site of axonal transport disruption, axonal cytoskeleton damage and putative axonal regeneration failure in a rat model of glaucoma. Acta neuropathol. 121, 737–751.
Cooper, M.L., Crish, S.D., Inman, D.M., Horner, P.J., Calkins, D.J., 2016 Dec 2. Early astrocyte redistribution in the optic nerve precedes axonopathy in the DBA/2J mouse model of glaucoma. Exp Eye Res. 150, 22–33.
Crish, S.D., Sappington, R.M., Inman, D.M., Horner, P.J., Calkins, D.J., 2010. Distal axonopathy with structural persistence in glaucomatous neurodegeneration. Proc. Natl. Acad. Sci. U. S. A. 107, 5196–5201.
Dai, C., Khaw, P.T., Yin, Z.Q., Li, D., Raisman, G., Li, Y., 2012. Structural basis of glaucoma: the fortified astrocytes of the optic nerve head are the target of raised intraocular pressure. Glia 60, 13–28.
Ebneter, A., Casson, R.J., Wood, J.P., Chidlow, G., 2010. Microglial activation in the visual pathway in experimental glaucoma: spatiotemporal characterization and correlation with axonal injury. Investig. Ophthalmol. Vis. Sci. 51, 6448–6460.
Ebneter, A., Casson, R.J., Wood, J.P., Chidlow, G., 2012. Estimation of axon counts in a rat model of glaucoma: comparison of fixed-pattern sampling with targeted sampling. Clin. Exp. Ophthalmol. 40, 626–633.
Gottanka, J., Kuhlmann, A., Scholz, M., Johnson, D.H., Lutjen-Drecoll, E., 2005. Pathophysiologic changes in the optic nerves of eyes with primary open angle and pseudoexfoliation glaucoma. Investig. Ophthalmol. Vis. Sci. 46, 4170–4181.
Harder, J.M., Fernandes, K.A., Libby, R.T., 2012. The Bcl-2 family member BIM has multiple glaucoma-relevant functions in DBA/2J mice. Sci. Rep. 2, 530.
Hernandez, M.R., 2000. The optic nerve head in glaucoma: role of astrocytes in tissue remodeling. Prog. Retin. Eye Res. 19, 297–321.
Howell, G.R., Libby, R.T., Jakobs, T.C., Smith, R.S., Phalan, F.C., Barter, J.W., Barbay, J.M., Marchant, J.K., Mahesh, N., Porciatti, V., Whitmore, A.V., Masland, R.H., John, S.W., 2007a. Axons of retinal ganglion cells are insulted in the optic nerve early in DBA/2J glaucoma. J. Cell Biol. 179, 1523–1537.
Howell, G.R., Libby, R.T., Marchant, J.K., Wilson, L.A., Cosma, I.M., Smith, R.S., Anderson, M.G., John, S.W., 2007b. Absence of glaucoma in DBA/2J mice homozygous for wild-type versions of Gpnmb and Tyrp1. BMC Genet. 8, 45.
Howell, G.R., Macalinao, D.G., Sousa, G.L., Walden, M., Soto, I., Kneeland, S.C., Barbay, J.M., King, B.L., Marchant, J.K., Hibbs, M., Stevens, B., Barres, B.A., Clark, A.F., Libby, R.T., John, S.W., 2011. Molecular clustering identifies complement and endothelin induction as early events in a mouse model of glaucoma. J. Clin. Investig. 121, 1429–1444.
Howell, G.R., Soto, I., Zhu, X., Ryan, M., Macalinao, D.G., Sousa, G.L., Caddle, L.B., MacNicoll, K.H., Barbay, J.M., Porciatti, V., Anderson, M.G., Smith, R.S., Clark, A.F., Libby, R.T., John, S.W., 2012. Radiation treatment inhibits monocyte entry into the optic nerve head and prevents neuronal damage in a mouse model of glaucoma. J. Clin. Investig. 122, 1246–1261.
Inman, D.M., Horner, P.J., 2007. Reactive nonproliferative gliosis predominates in a chronic mouse model of glaucoma. Glia 55, 942–953.
Inman, D.M., Lupien, C.B., Horner, P.J., 2011. Manipulating glia to protect retinal ganglion cells in glaucoma. In: Gunvant, P. (Ed.), Glaucoma – Current Clinical Research Aspects. InTech, Rijeka, Croatia, ISBN 978-953-307-263-0.
Inman, D.M., Sappington, R.M., Horner, P.J., Calkins, D.J., 2006. Quantitative correlation of optic nerve pathology with ocular pressure and corneal thickness in the DBA/2 mouse model of glaucoma. Investig. Ophthalmol. Vis. Sci. 47, 986–996.
Isaacs, J., Mallu, S., Batchelor, M., 2014. Modification of commercially available image analysis software for semi-automated qualitative analysis of axon regeneration and myelination in the rat sciatic nerve. J. Neurosci. Methods 233, 45–49.
Jia, L., Cepurna, W.O., Johnson, E.C., Morrison, J.C., 2000. Patterns of intraocular pressure elevation after aqueous humor outflow obstruction in rats. Investig. Ophthalmol. Vis. Sci. 41, 1380–1385.
John, S.W., Smith, R.S., Savinova, O.V., Hawes, N.L., Chang, B., Turnbull, D., Davisson, M., Roderick, T.H., Heckenlively, J.R., 1998. Essential iris atrophy, pigment dispersion, and glaucoma in DBA/2J mice. Investig. Ophthalmol. Vis. Sci. 39, 951–962.
Johnson, E.C., Jia, L., Cepurna, W.O., Doser, T.A., Morrison, J.C., 2007. Global changes in optic nerve head gene expression after exposure to elevated intraocular pressure in a rat glaucoma model. Investig. Ophthalmol. Vis. Sci. 48, 3161–3177.
Jonas, J.B., Schmidt, A.M., Muller-Bergh, J.A., Naumann, G.O., 1995. Optic nerve fiber count and diameter of the retrobulbar optic nerve in normal and glaucomatous eyes. Graefes Arch. Clin. Exp. Ophthalmol. 233, 421–424.
Joos, K.M., Li, C., Sappington, R.M., 2010. Morphometric changes in the rat optic nerve following short-term intermittent elevations in intraocular pressure. Investig. Ophthalmol. Vis. Sci. 51, 6431–6440.
Libby, R.T., Anderson, M.G., Pang, I.H., Robinson, Z.H., Savinova, O.V., Cosma, I.M., Snow, A., Wilson, L.A., Smith, R.S., Clark, A.F., John, S.W., 2005a. Inherited glaucoma in DBA/2J mice: pertinent disease features for studying the neurodegeneration. Vis. Neurosci. 22, 637–648.
Libby, R.T., Li, Y., Savinova, O.V., Barter, J., Smith, R.S., Nickells, R.W., John, S.W., 2005b. Susceptibility to neurodegeneration in a glaucoma is modified by Bax gene dosage. PLoS Genet. 1, 17–26.
Lye-Barthel, M., Sun, D., Jakobs, T.C., 2013. Morphology of astrocytes in a glaucomatous optic nerve. Investig. Ophthalmol. Vis. Sci. 54, 909–917.
Mabuchi, F., Aihara, M., Mackey, M.R., Lindsey, J.D., Weinreb, R.N., 2003. Optic nerve

damage in experimental mouse ocular hypertension. Investig. Ophthalmol. Vis. Sci. 44, 4321–4330.
Magnus, T., Coksaygan, T., Korn, T., Xue, H., Arumugam, T.V., Mughal, M.R., Eckley, D.M., Tang, S.C., Detolla, L., Rao, M.S., Cassiani-Ingoni, R., Mattson, M.P., 2007. Evidence that nucleocytoplasmic Olig2 translocation mediates brain-injury-induced differentiation of glial precursors to astrocytes. J. Neurosci. Res. 85, 2126–2137.
Marina, N., Bull, N.D., Martin, K.R., 2010. A semiautomated targeted sampling method to assess optic nerve axonal loss in a rat model of glaucoma. Nat. Protoc. 5, 1642–1651.
May, C.A., Mittag, T., 2006. Optic nerve degeneration in the DBA/2NNia mouse: is the lamina cribrosa important in the development of glaucomatous optic neuropathy? Acta Neuropathol. 111, 158–167.
Morrison, J.C., Moore, C.G., Deppmeier, L.M., Gold, B.G., Meshul, C.K., Johnson, E.C., 1997. A rat model of chronic pressure-induced optic nerve damage. Exp. Eye Res. 64, 85–96.
Nakazawa, T., Nakazawa, C., Matsubara, A., Noda, K., Hisatomi, T., She, H., Michaud, N., Hafezi-Moghadam, A., Miller, J.W., Benowitz, L.I., 2006. Tumor necrosis factor-alpha mediates oligodendrocyte death and delayed retinal ganglion cell loss in a mouse model of glaucoma. J. Neurosci. Off. J. Soc. Neurosci. 26, 12633–12641.
Naskar, R., Wissing, M., Thanos, S., 2002. Detection of early neuron degeneration and accompanying microglial responses in the retina of a rat model of glaucoma. Investig. Ophthalmol. Vis. Sci. 43, 2962–2968.
Nickells, R.W., Howell, G.R., Soto, I., John, S.W., 2012. Under pressure: cellular and molecular responses during glaucoma, a common neurodegeneration with axonopathy. Annu. Rev. Neurosci. 35, 153–179.
Nuschke, A.C., Farrell, S.R., Levesque, J.M., Chauhan, B.C., 2015. Assessment of retinal ganglion cell damage in glaucomatous optic neuropathy: axon transport, injury and soma loss. Exp. Eye Res. 141, 111–124.
Pelzel, H.R., Schlamp, C.L., Waclawski, M., Shaw, M.K., Nickells, R.W., 2012. Silencing of Fem1cR3 gene expression in the DBA/2J mouse precedes retinal ganglion cell death and is associated with histone deacetylase activity. Investig. Ophthalmol. Vis. Sci. 53, 1428–1435.
Qu, J., Jakobs, T.C., 2013. The time course of gene expression during reactive gliosis in the optic nerve. PloS One 8, e67094.
Quigley, H.A., 2011. Glaucoma. Lancet 377, 1367–1377.
Quigley, H.A., Addicks, E.M., Green, W.R., 1982. Optic nerve damage in human glaucoma. III. Quantitative correlation of nerve fiber loss and visual field defect in glaucoma, ischemic neuropathy, papilledema, and toxic neuropathy. Arch. Ophthalmol. 100, 135–146.
Radius, R.L., Pederson, J.E., 1984. Laser-induced primate glaucoma. II. Histopathology. Arch. Ophthalmol. 102, 1693–1698.
Reynaud, J., Cull, G., Wang, L., Fortune, B., Gardiner, S., Burgoyne, C.F., Cioffi, G.A., 2012. Automated Quantification of Optic Nerve Axons in Primate Glaucomatous and Normal Eyes–method and Comparison to Semi-Automated Manual Quantification.
Salinas-Navarro, M., Alarcon-Martinez, L., Valiente-Soriano, F.J., Jimenez-Lopez, M., Mayor-Torroglosa, S., Aviles-Trigueros, M., Villegas-Perez, M.P., Vidal-Sanz, M., 2010. Ocular hypertension impairs optic nerve axonal transport leading to progressive retinal ganglion cell degeneration. Exp. Eye Res. 90, 168–183.
Sandell, J.H., Peters, A., 2002. Effects of age on the glial cells in the rhesus monkey optic nerve. J. Comp. Neurol. 445, 13–28.
Sappington, R.M., Carlson, B.J., Crish, S.D., Calkins, D.J., 2010. The microbead occlusion model: a paradigm for induced ocular hypertension in rats and mice. Investig. Ophthalmol. Vis. Sci. 51, 207–216.
Sappington, R.M., Pearce, D.A., Calkins, D.J., 2003. Optic nerve degeneration in a murine model of juvenile ceroid lipofuscinosis. Investig. Ophthalmol. Vis. Sci. 44, 3725–3731.
Schlamp, C.L., Li, Y., Dietz, J.A., Janssen, K.T., Nickells, R.W., 2006. Progressive ganglion cell loss and optic nerve degeneration in DBA/2J mice is variable and asymmetric. BMC Neurosci. 7, 66.
Scholz, M., Buder, T., Seeber, S., Adamek, E., Becker, C.M., Lutjen-Drecoll, E., 2008. Dependency of intraocular pressure elevation and glaucomatous changes in DBA/2J and DBA/2J-Rj mice. Investig. Ophthalmol. Vis. Sci. 49, 613–621.
Schuettauf, F., Rejdak, R., Walski, M., Frontczak-Baniewicz, M., Voelker, M., Blatsios, G., Shinoda, K., Zagorski, Z., Zrenner, E., Grieb, P., 2004. Retinal neurodegeneration in the DBA/2J mouse-a model for ocular hypertension. Acta neuropathol. 107, 352–358.
Smith, R.S., Zabaleta, A., John, S.W., Bechtold, L.S., Ikeda, S., Relyea, M., Sundberg, J., Liu, C.-Y., Kao, W., 2002. General and specific histopathology. In: Smith, R.S. (Ed.), Systemic Evaluation of the Mouse Eye. CRC Press, New York, pp. 265–297.
Sofroniew, M.V., 2009. Molecular dissection of reactive astrogliosis and glial scar formation. Trends Neurosci. 32, 638–647.
Son, J.L., Soto, I., Oglesby, E., Lopez-Roca, T., Pease, M.E., Quigley, H.A., Marsh-Armstrong, N., 2010. Glaucomatous optic nerve injury involves early astrocyte reactivity and late oligodendrocyte loss. Glia 58, 780–789.
Soto, I., Oglesby, E., Buckingham, B.P., Son, J.L., Roberson, E.D., Steele, M.R., Inman, D.M., Vetter, M.L., Horner, P.J., Marsh-Armstrong, N., 2008. Retinal ganglion cells downregulate gene expression and lose their axons within the optic nerve head in a mouse glaucoma model. J. Neurosci. Off. J. Soc. Neurosci. 28, 548–561.
Soto, I., Pease, M.E., Son, J.L., Shi, X., Quigley, H.A., Marsh-Armstrong, N., 2011. Retinal ganglion cell loss in a rat ocular hypertension model is sectorial and involves early optic nerve axon loss. Investig. Ophthalmol. Vis. Sci. 52, 434–441.
Sun, D., Jakobs, T.C., 2012. Structural remodeling of astrocytes in the injured CNS. Neurosci. Rev. J. Bring. Neurobiol. Neurol. Psychiatr. 18, 567–588.
Sun, D., Lye-Barthel, M., Masland, R.H., Jakobs, T.C., 2009. The morphology and spatial arrangement of astrocytes in the optic nerve head of the mouse. J. Comp. Neurol. 516, 1–19.
Teixeira, L.B., Buhr, K.A., Bowie, O., Duke, F.D., Nork, T.M., Dubielzig, R.R., McLellan, G.J., 2014. Quantifying optic nerve axons in a cat glaucoma model by a semi-automated targeted counting method. Mol. Vis. 20, 376–385.
Templeton, J.P., Struebing, F.L., Lemmon, A., Geisert, E.E., 2014. ImagePAD, a novel counting application for the Apple iPad, used to quantify axons in the mouse optic nerve. Exp. Eye Res. 128, 102–108.
Verkhratsky, A., Parpura, V., Pekna, M., Pekny, M., Sofroniew, M., 2014. Glia in the pathogenesis of neurodegenerative diseases. Biochem. Soc. Trans. 42, 1291–1301.
Vidal-Sanz, M., Salinas-Navarro, M., Nadal-Nicolas, F.M., Alarcon-Martinez, L., Valiente-Soriano, F.J., de Imperial, J.M., Aviles-Trigueros, M., Agudo-Barriuso, M., Villegas-Perez, M.P., 2012. Understanding glaucomatous damage: anatomical and functional data from ocular hypertensive rodent retinas. Prog. Retin. Eye Res. 31, 1–27.
Yang, Q., Cho, K.S., Chen, H., Yu, D., Wang, W.H., Luo, G., Pang, I.H., Guo, W., Chen, D.F., 2012. Microbead-induced ocular hypertensive mouse model for screening and testing of aqueous production suppressants for glaucoma. Investig. Ophthalmol. Vis. Sci. 53, 3733–3741.